A&A 409, 309–316 (2003)
DOI: 10.1051/0004-6361:20031097

Astronomy & Astrophysics

Relative timing of electron acceleration and injection at solar flares: A case study

H. T. Claßen, G. Mann, A. Klassen, and H. Aurass

Astrophysikalisches Institut Potsdam, An der Sternwarte 16, 14482 Potsdam, Germany

Received 5 February 2003 / Accepted 30 June 2003

Abstract. Multiple-wavelength observations of a C-class solar flare and in situ measurements of high-energy electrons at 1 AU are combined for a detailed analysis of the relative timing of solar electromagnetic emission and high-energy electron injection. The primary energy release for the C8.0 flare on 2002 June 02 (10:05–10:30 UT) is studied using hard X-ray data of the Reuven Ramaty High Energy Solar Spectroscopic Imager (RHESSI). The propagation of disturbances through the solar corona and interplanetary space is investigated by means of dynamic radio spectra obtained by ground-based observatories (Ondřejov, Czech Republic, and Potsdam, Germany). The time sequence of these indirect manifestations of highly energetic electrons is correlated with the extrapolated injection time obtained by a transit time analysis from Sun to Earth using the enhancement in the 27–182 keV electron intensity observed at the *Wind* spacecraft. This back-mapping of high-energy electrons shows that the particles are injected roughly 18 min after the first hard X-ray maximum. Almost at the same time there are observations of metric type II and IV radio bursts indicating the presence of a coronal shock wave and a moving plasmoid whose kinematics are analysed by means of dynamic radio spectra and radio images from the Nançay Radioheliograph (France). Implications for possible acceleration and injection scenarios are discussed.

Key words. Sun: flares – Sun: X-rays, gamma rays – Sun: radio radiation – Sun: particle emission – shock waves – acceleration of particles

1. Introduction

Highly energetic electrons generated during solar flares manifest themselves indirectly via the excitation of electromagnetic waves and/or can be measured in situ after their injection on magnetic field lines connecting the solar release site and appropriate detectors. In the sixties Wild et al. (1963) and de Jager (1969) claimed that (sub)-relativistic protons and electrons are accelerated during the second phase of a flare associated with characteristic radio emission, so-called type II and type IV radio bursts.

Type II radio bursts are radio signatures of coronal shock waves. The electromagnetic waves are generated by energetic electron populations accelerated at the shock giving rise to the production of Langmuir turbulence (e.g., Nelson & Melrose 1985). In dynamic radio spectra (cf. Fig. 1) type II bursts appear as narrow bands of enhanced radio emission drifting slowly from high to low frequencies. The different bands of electromagnetic emission are due to the interaction of the Langmuir waves with low frequency plasma waves (fundamental band) or due to Langmuir wave – Langmuir wave interaction (harmonic band). Type IV radio bursts appear as broad band continuum emission – sometimes with fine structures. Type IV bursts are generated by highly energetic electrons in closed magnetic field structures, e.g., loops or moving plasmoids (e.g., Stewart 1985).

In principal, electron acceleration to high energies can be achieved by at least two different processes which can act independently of each other. The first mechanism is associated with magnetic reconnection (e.g., Priest 1981). The acceleration takes place during the impulsive flare phase on a temporal scale of $\leq 10^{-2}$ s (Sturrock et al. 1984) in a region of $\geq (300\ \mathrm{km})^2$ (de Jager et al. 1987). The precipitation into denser regions of the solar atmosphere produces hard X-ray bursts, optical, and UV emission (e.g., Heyvaerts 1981). Electrons escaping on open field lines into the interplanetary medium can produce type III solar radio bursts (e.g., Suzuki & Dulk 1985).

The second acceleration process is associated with coronal shock waves. Many authors consider a so-called first order Fermi acceleration (e.g., Forman & Webb 1985). For this kind of electron acceleration by multiple reflections at magnetic field fluctuations in the up- and downstream region it is essential that the electrons have been pre-accelerated in order to be picked up in this process. Seed populations of pre-accelerated particles in the first order Fermi process are one of the reasons for considering separate phases for high-energy electron production (e.g., Bai & Ramaty 1979; Bai & Dennis 1985). It should be mentioned that the shock itself can possibly generate the seed population of electrons above the injection energy. Thus it has been pondered about shock drift

Send offprint requests to: H. T. Claßen,
e-mail: tclassen@aip.de

acceleration (e.g., Armstrong et al. 1985) as a mechanism for pre-acceleration (e.g., Melrose 1994). A strong indication for nearly relativistic electrons accelerated at rising shocks was recently given by Mann et al. (2001), Klassen et al. (2002), and Simnett et al. (2002).

Another reason for considering two acceleration phases is based on the analysis of the relative timing of solar electromagnetic emissions and the injection of high-energy electrons. Thus Krucker et al. (1999) and Haggerty & Roelof (2002) analysed the injection time of near-relativistic electrons observed by in situ measurements aboard the *Wind* and ACE (Advanced Composition Explorer) spacecrafts at 1 AU. Both research groups found populations of 25–300 keV electrons which have been injected typically 10 min after the electromagnetic fingerprints of the impulsive flare phase (type III bursts or microwave bursts). One possible explanation for this considerable delay are storage effects (Švestka 1976). Krucker et al. (1999) discuss the delay in the context of high altitude Moreton- or EIT waves travelling from the flare site to the escape region. Haggerty & Roelof (2002) and Simnett et al. (2002) favor electron acceleration at shock waves.

The analysis carried out in the present paper starts with a synopsis of multiple-wavelength observations of a C8.0 flare on 2002 June 02 from 10:05 to 10:30 (Fig. 1). The primary energy release is studied in hard X-rays (6–100 keV, RHESSI) and microwaves (0.8–4.5 GHz, observatory Ondřejov). The propagation of disturbances – electron beams, shock waves – through the solar corona is analysed via dynamic radio radio spectra in the 40–800 MHz range (observatory Potsdam). Finally, the high-energy electron intensity near Earth is taken from the 3D Plasma and Energetic Particle experiment on *Wind* spacecraft (*Wind*/3-DP).

The reason for going ahead with a detailed case study – in contrast to the statistical approaches carried out by Krucker et al. (1999) and Haggerty & Roelof (2002) – lies in the complexity of the studied phenomena. We chose an event occurring at the western limb (S20W61), i.e., we expect a direct magnetic connection between the spacecraft and the Sun. Moreover, the radio observations allow the velocities of electron beams (type IIIs) and the coronal shock wave (type II) to be determined. We also use radio images from the Nançay Radioheliograph (NRH) (cf. Fig. 2) for a localisation of the type IV source which turns out to be a moving plasmoid.

In the next section we will briefly describe the instruments. Furthermore, we present the results for the electron beam, shock wave, and plasmoid kinematics. The discussion of possible injection and acceleration scenarios is carried out in Sect. 3. We will firstly analyse the possibility of electron acceleration during the primary energy release phase producing hard X-ray peaks and microwave bursts. Secondly, we want to take into account the possibility of energy storage and release connected with the type IV source. Finally, we will consider the possibility of electron acceleration at a rising shock considering also the development of shock waves in the solar corona with respect to the change of plasma parameters during the rise of the shock.

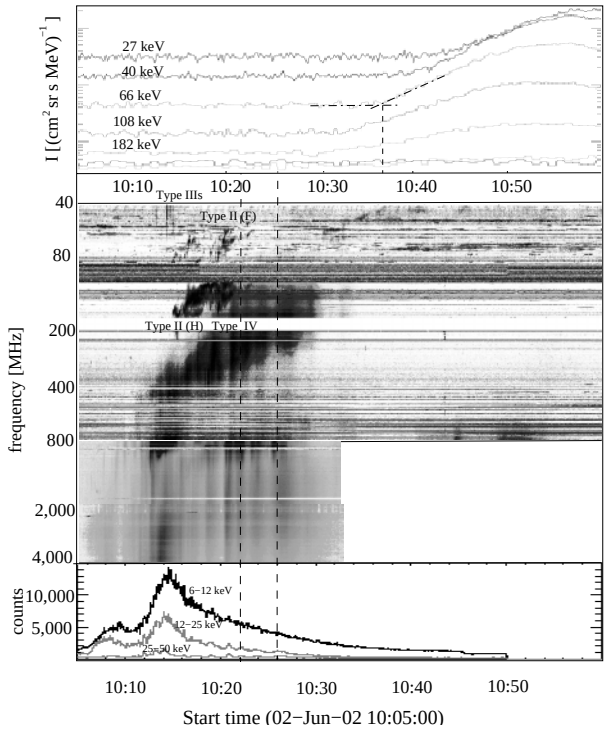

Fig. 1. Synopsis of the 2-June-2002 C8.0 flare showing the energy release in hard X-rays (RHESSI), manifestations of high-energy electrons in micro- and meter-waves radio observations (4.5–0.8 GHz, observatory Ondřejov; 800–40 MHz, observatory Potsdam), and the enhancement of high-energy electron intensity near Earth (*Wind*/3-DP). The dashed-dotted lines in the upper panel sketch how the arrival time at 1 AU is determined. The vertical dashed lines across the lightcurves and spectra indicate the relative electron injection time at the Sun.

2. Data analysis

Figure 1 shows a synopsis of the flare on June 02 covering both electromagnetic emission and high-energy electron intensity from 10:05–11:00 UT. The RHESSI lightcurves indicate the primary energy release in the lower corona, and the different radio observations enable a tracing of transients moving through the corona. In order to relate these observations to the in situ measurements of high-energy electrons at *Wind* one should keep in mind that both electromagnetic waves and accelerated electrons are travelling from the Sun to the appropriate detectors with different velocities. All measurements in Fig. 1 refer to the actual time at the particular detectors, and only the dashed lines across the lightcurves and spectra account for the differences in the propagation time.

The event displayed in Fig. 1 is part of an event-catalog combining radio observations of coronal shock waves – type II bursts – with hard X-ray lightcurves. The catalog comprises the type II bursts observed by the radio spectral polarimeter of the Astrophysikalisches Institut Potsdam (Mann et al. 1992) since the launch of the RHESSI spacecraft on 2002 Feb. 5. This list presently consists of roughly 50 type II bursts (see `http://www.aip.de/People/AKlassen/type_II_list_2002.html`) observed in dynamic radio spectra from 40–800 MHz with a time resolution of 0.1 s. First results on

two events contained in this catalog have been published by Claßen et al. (2003).

The RHESSI instrument (Lin et al. 2002) utilizes bi-grid rotating modulation collimators and cooled germanium detectors to observe X- and γ-rays from roughly 3 keV to 20 MeV. Via a Fourier transformation RHESSI provides a hard X-ray imaging spectroscopy with an angular resolution down to 2 arcsec, a time resolution down to tens of ms, and roughly 1 keV energy resolution. The lower panel of Fig. 1 shows the X-ray flux (counts) measured by the RHESSI spacecraft working in the first attenuator stage. A further analysis showed that there is only a very weak X-ray emission above 50 keV. In the low energy channels there are two maxima, the first around 10:08 UT and second one with even higher count rates around 10:14 UT. Furthermore, there are several minor peaks – clearly distinguished in the 25–50 keV channel – at roughly 10:12, 10:13, 10:14, 10:19, 10:21 UT, and some smaller bumps around 10:24 and 10:26 UT. We zoom in on this energy range in Figs. 4 and 5.

Looking back at Fig. 1 it can be seen that the meter-wave spectra (40–800 MHz) are supplemented by the cm- to dm-wave spectra from 800–4500 MHz recorded by the observatory in Ondřejov (Jiřička et al. 1993, data by courtesy of M. Karlický). Thus, the broad band radio observations from 40–4500 MHz enable a tracing of the various radio sources from the lower corona almost into interplanetary space.

Assuming a plasma emission process for the generation of the meter-wave bursts (e.g., Melrose 1994) the emission frequency is proportional to the square-root of the electron particle number density and the bursts' drift rates allow for the determination of the exciter velocity. In solar radio astronomy it is usual to adopt enhanced standard models to describe the changes in the electron particle number density from the lower corona to interplanetary space. The reason for choosing enhancement factors in comparison with the standard models lies in the fact that the particle number above active regions is both spatially and temporary increased. This leads to an uncertainty in the order of 35% for heights and velocities derived from dynamic radio spectra (e.g., Claßen & Aurass 2002). In our study we use a twofold Newkirk model (Newkirk 1961) for the meter-wave observations.

The various types of meter wave bursts observed during our event are marked in Fig. 1. There are several slow- (type II and IV) and fast-drifting (type III) emission features. The type II emission consists of a weak patchy fundamental emission (F) and a stronger harmonic emission (H) starting at 170 MHz at 10:15 UT with a frequency drift rate of roughly –0.23 MHz s^{-1}. The emission stops about 10:22 UT at 50 MHz (fundamental band) but at 10:30 UT there is again type II emission at 60 MHz – likely the continuation of the previously recorded harmonic band – lasting until 10:38 UT. Using a twofold Newkirk model we obtain that the radio emission starts at roughly 0.4 $R_\odot$ ($R_\odot$ solar radius) above the photosphere with a radial source speed of 540 km s^{-1} and the emission ends at roughly 0.7 $R_\odot$. Assuming that the type II emission at 10:30 UT is harmonic emission we obtain a corresponding height of roughly 1.1 $R_\odot$ above the photosphere. The type II emission is accompanied by strong type IV emission recorded between approximately 10:11 and 10:30 UT from 800 to 100 MHz. The broad band continuum emission shows fast drifting fine structures, especially at the lower edge, i.e., at the high-frequency end.

Concerning fast drifting features, the Potsdam instrument recorded the first type III bursts between 400 and 300 MHz at 10:12:05 UT (not visible in Fig. 1). Due to the narrow bandwidth of these bursts we can only estimate the driver speed and we obtain a velocity of roughly 30 000 km s^{-1}, i.e. $\beta = v/c = 0.1$ (c, velocity of light). There is another group of type III bursts – this time visible in Fig. 1 – starting at 10:14:20 UT below 70 MHz with a drift rate of –5.1 MHz s^{-1} at the 50 MHz plasma level corresponding to an exciter velocity of roughly 40 000 km ($\beta = 0.13$). A further inspection of the radio receivers aboard the *Wind* spacecraft (*Wind*/WAVES) showed a continuation of these bursts to lower frequencies indicating the presence of electron beams on open field lines.

Figure 2 shows the location of hard X-ray, type II, and type IV sources at different times. The hard X-ray source is located in the south-west of the solar disk (Solar $X = 770''$ and Solar $Y = -330''$, i.e., S20W61) as can be seen from the zoomed RHESSI image in the upper part of Fig. 2. The image was taken in the energy range between 25–50 keV around 10:14 UT with an integration time of 36.88 s corresponding to 9 spacecraft rotations. A weak double source structure with roughly 10 arcsec distance can be seen.

The radio images from the Nançay Radioheliograph (Kerdraon & Delouis 1999, data by courtesy of the NRH Group) show structures with a size of several arcminutes. The contour plot indicates four intensity levels from 20 to 80% for the type IV source at 432 MHz at one specific time (10:12:01 UT). For all other times the size of the circles indicates the observation frequency (from 432–164 MHz) while the position of the circles shows the centroid position of the radio source. Figure 2 shows the 8 radio source locations at 432 MHz with one minute time difference each, and 3 source positions at 327 MHz and 164 MHz, respectively. The integration time for each image is 10 s.

The squares show the position of the type II source at five different times at 164 MHz, i.e., the location of the harmonic band is displayed. The hatched square at 10:15:01 UT shows the position of the so-called "arc" structure – visible in dynamic radio spectra – preceding the type II burst. This emission feature is sometimes observed at the beginning of the type II emission. In the cases studied by Klassen et al. (1999) the "arc" sources are located near the summit of active region loops.

The filled symbols indicate the radio source positions of the type IV (two circles) and the type II (square) burst at one specific time (10:15:31 UT). From this representation it can be seen that the type II source is clearly running ahead of the type IV source. Thus it is very likely that we are observing a moving plasmoid driving a bow shock in front of it. The NRH radio observations revealed a type IV source velocity of 495 km s^{-1} at 432 MHz, 465 km s^{-1} from 432 to 327 MHz, and 432 km s^{-1} from 432 to 164 MHz, respectively. These velocities are in good agreement with the estimation of the type II source speed of 540 km s^{-1} obtained from the drift rate in the dynamic radio spectrum.

As seen in Fig. 2, the event on June 2, 2002 is located at the western solar limb and thus one can expect a magnetic

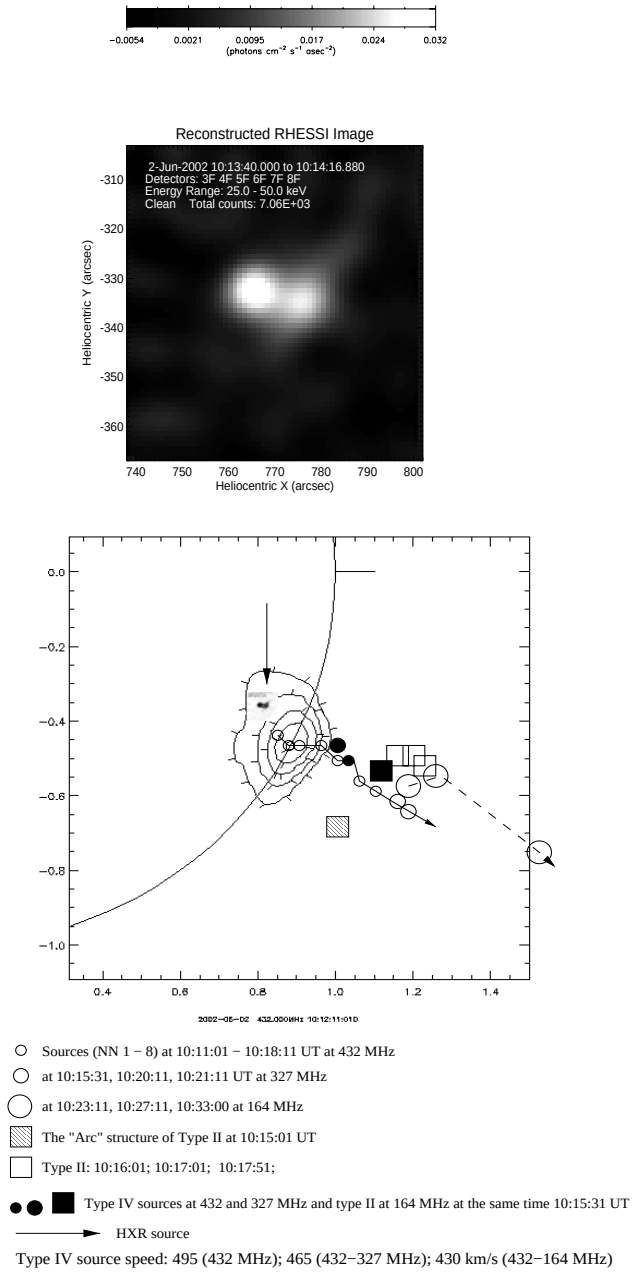

Fig. 2. Hard X-ray (RHESSI) and radio sources (NRH) of the flare on June 2, 2002. The figure shows the location of the hard X-ray source (25.0–50.0 keV) around 10:14 UT and the location of the centroid of the radio sources of the type II and IV burst at different times (circles and squares). For the observed frequencies and times see the legend below indicating also the source velocity. (The filled circles are included in the temporal sequences labelled by open symbols. The filled circles and the filled square are used to accentuate the location at one specific time.) The contour plot shows four intensity levels at 432 MHz from 20 to 80% indicating a spatial resolution of several arc minutes. The arrow points at the hard X-ray source (HXR) enlarged in the upper part.

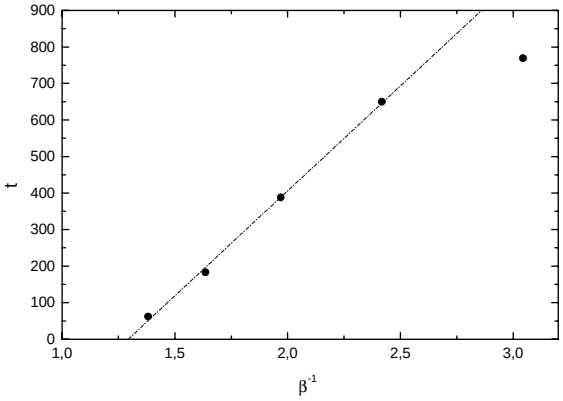

Fig. 3. Arrival time $t_{\rm AU}$ of high-energy electrons at *Wind* as function of the inverse velocity. The origin of the time axis is arbitrarily fixed at 10:30 UT. The straight dotted line is a linear fit to the observations at $\beta^{-1} = 1.381,\ 1.634,\ 1.972$, and 2.421 ($\beta = v/c$). The electrons measured at low energies, i.e., $\beta^{-1} = 3.049$, are excluded.

connection between Sun and Earth. The upper panel of Fig. 1 shows the onset of an impulsive electron event at 1 AU using the *Wind*/3-DP instrument. The characteristics of these kinds of events are specified in Krucker et al. (1999). The instrument is described in detail by Lin et al. (1995) and allows full three-dimensional measurements of electron and ion distributions. The *Wind*/3-DP data were provided by the Wind 3D Plasma and Energetic Particle Investigation team (R. P. Lin, PI) at the University of California, Berkeley.

The arrival time of the high-energy electrons recorded by the *Wind*/3-DP experiment enables the estimation of the coronal injection time. The method used here follows the approach described by Krucker et al. (1999). The arrival time $t_{\rm AU}$ at 1 AU is determined from the background-subtracted time profile of the electron intensity in the analysed energy channel. This procedure is sketched in Fig. 1 by the dashed-dotted lines for the electrons in the 66 keV energy channel. $t_{\rm AU}$ is the point of time where the two lines smoothing the noise and fitting the intensity increase intersect.

The electron injection time t_0 is given by $t_0 = t_{\rm AU} - L/v$ with L as path length from the release site on the Sun to the detector and v as particle velocity. Taking into consideration that the recorded electrons are observed in energy bands with a finite width we must specify the most probable velocity of the electrons in each energy bin. In accordance with Krucker (Krucker et al. 1999, and private communication) we choose the following values for the kinetic energy ϵ and relativistic velocity $\beta = v_{\rm rel}(\epsilon)/c$: $\epsilon_1 = 30$ keV ($\beta_1 = 0.328$), $\epsilon_2 = 50$ keV ($\beta_2 = 0.413$), $\epsilon_3 = 82$ keV ($\beta_3 = 0.507$), $\epsilon_4 = 135$ keV ($\beta_4 = 0.612$), and $\epsilon_5 = 230$ keV ($\beta_5 = 0.724$). Figure 3 shows the arrival time $t_{\rm AU}$ of highly energetic electrons observed at *Wind* as function of the inverse velocities β_i ($i = 1, ..., 5$). The origin of the time axis is arbitrarily fixed at 10:30 UT. Krucker et al. (1999) describe two possibilities to determine the electron injection time t_0. The first method comprises a linear fit to the data in the different energy bins where the slope corresponds to the path length L. From the fit displayed in Fig. 3 we obtain a path length of $L = 247.6\ R_\odot$ (1.15 AU). Beyond, it can be seen that the electrons with the lowest energy deviate from an almost linear behaviour of the electrons observed at higher energies. This effect was already discussed by Krucker et al. (1999) considering electron populations with a different

coronal origin. But it might also be that the 30 keV channel is affected by the higher energy channels. Therefore we fitted only the electrons in the high-energy bins from 50 to 230 keV and obtain a coronal injection at $t_0 = -743$ s (with respect to 10:30 UT). In order to compare the injection time with the observations of electromagnetic waves at or near Earth we have to take into account their propagation time from Sun to Earth. Thus, we obtain a relative electron injection at 10:26 UT keeping in mind that the actual injection took place roughly 8 min (496 s) earlier.

The second method utilizes an explicit value of the path length L which can be estimated assuming an electron propagation along the interplanetary magnetic field given by the Parker spiral. The length of the Parker spiral depends on the solar wind speed $v_{\rm sw}$ and the duration of the solar rotation T_r. Choosing a velocity of $v_{\rm sw} = 400\ {\rm km\,s^{-1}}$ as appropriate value for the event under consideration and $T_r = 26$ days we obtain a path length of $L = 1.16$ AU. Thus, both methods provide (almost) the same result for the path length. Using this value of L we obtain a relative injection taking place at 10:26 UT for the electrons in the four high-energy channels. Assuming a different electron population observed at 30 keV we obtain a relative injection at 10:22 UT. These times are indicated by the vertical dashed lines across the spectra and lightcurves in Fig. 1.

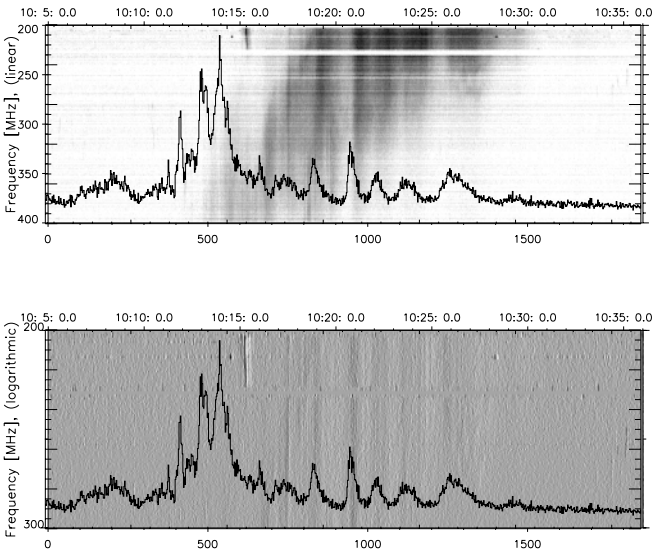

Fig. 4. Temporal variation of the RHESSI count rates in the 25–50 keV energy channel (black line) and solar radio emission between 200 and 400 (300) MHz (observatory Potsdam). The dynamic radio spectrum in the upper panel shows the relative intensity $I(f,t)$ of the moving type IV radio burst visible in Figs. 1 and 2 from 200–400 MHz. The lower panel shows the first temporal derivative $\partial I/\partial t$ from 200–300 MHz. The abscissae show the time (UT) in hh:mm:ss notation (upper labels) and the time elapsed since 10:05:00 UT in seconds (lower labels).

3. Discussion

In order to discuss the relative timing of electromagnetic emission and the injection of high-energy electrons Figs. 4 and 5 show the decisive parts of the dynamic radio spectra displayed in Fig. 1.

Figure 4 combines the radio flux between 200 and 400 MHz (300 MHz in the lower panel) with the hard X-ray count rates in the 25–50 keV energy channel. The hard X-ray flux in this energy range consists of a series of well distinguished peaks and it can be seen that the minor peaks recorded after 10:15 UT are associated with the fast drifting emission features of the lower, i.e., high frequency edge of the type IV burst. The temporal coincidence is clearly visible in the lower panel of Fig. 4 showing the first temporal derivative of the radio intensity $I(f,\ t)$ between 200 and 300 MHz. Thus it can be seen that the hard X-ray peaks coincide with the steepest gradient in the temporal behaviour of the recorded radio spectra. This means that the hard X-ray peaks mark the onset of the type IV associated fine structures starting with a sharp increase in the radio flux followed by a smooth decrease.

A close temporal association between hard X-ray and radio emission can also be seen in the synoptic plots displayed in Fig. 5. For the high frequency radio spectra, the range of temporal coincidence is extended over the whole period from 10:10 to 10:30 UT. That is to say that the high frequency spectra also show emission features temporally associated with the major hard X-ray peaks around 10:14 UT while the corresponding plots of Fig. 4 lacked this coincidence. But it is likely that radio emission in the frequency range between 0.8 and 2.0 GHz around 10:14 UT (upper panel of Fig. 5) is part of the type IV burst observed in the meter-waves (cf. Fig. 1). Thus we can conclude that the temporal coincidence between hard X-ray and radio emission is very close for the fast drifting fine structures of the type IV burst.

The coincidence between hard X-ray and type II radio emission seems to be not very close. But one has to keep in mind that small fluctuations caused by the shock may have been masked by the high background flux produced by the flare. This becomes plain looking e.g. at the reversely drifting burst between 200 and 250 MHz recorded shortly after 10:15 UT (Fig. 4). The burst is recorded at the onset of the harmonic type II emission fully visible in Fig. 1, and this indicates that an electron beam is moving towards the photosphere. While it is likely that these electrons have been accelerated at the shock wave it can be seen from Fig. 4 that there no obvious coincidence in hard X-rays.

With respect to the high-energy electrons detected at *Wind* Figs. 4 and 5 also show a close temporal correlation. Assuming that the 30 keV electrons were released around 10:22 UT and the higher energetic electrons around 10:26 UT we can see that for both times there are peaks in the hard X-ray emission and fast drifting emission features in the radio spectra. But it is also visible that there is a number of other hard X-ray peaks – most of them with higher count rates – at different times. RHESSI recorded a series of more or less well-defined peaks with a temporal distance of roughly one minute.

Due to the uncertainties in our estimation of the arrival time AT 1 AU – in the order of ±30 s – we cannot exclude an injection associated with one of these other minor peaks or between two peaks but it seems very unlikely that the electron

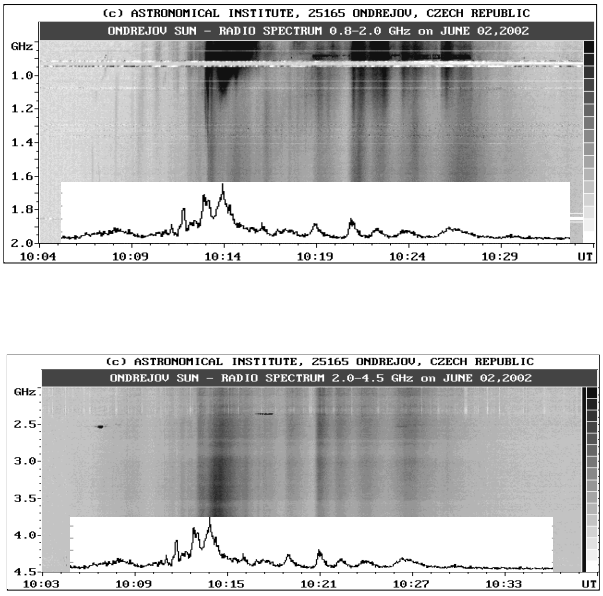

Fig. 5. Temporal variation of the RHESSI count rates in the 25–50 keV energy channel (black on white insertion) and intensity $I(f,t)$ of solar radio emission from 0.8–2.0 GHz (upper panel) and 2.0–4.5 GHz (lower panel) (Ondřejov observatory).

injection on a field line connected with *Wind* is temporally correlated with the major peaks recorded around 10:14 UT. In any case one should realise that there is still hard X-ray and microwave activity while the electron injection takes place, i.e., the reconnection process is still in progress. From this point of view the event of June 2 differs from the events studied by Klassen et al. (2002) who selected events with no microwave or hard X-ray bursts around the estimated electron injection time.

A direct evidence of high-energy electrons on open field lines can be deduced from the type III bursts recorded at 10:14:20 UT below 70 MHz (see Fig. 1). A further inspection of *Wind*/WAVES radio data showed a continuation of these bursts to longer wavelengths indicating that there are electron beams ($\beta \approx 0.13$) entering interplanetary space. A further analysis of RHESSI images showed that the hard X-ray source position is not changing significantly from 10:05–10:30 UT. Thus one would expect a magnetic connection between flare site and *Wind* during the whole flare on one hand but on the other hand all electrons detected in situ at *Wind* have been injected after the disappearance of the type II emission. The 30 keV electrons are released immediately afterwards, i.e., around 10:22 UT, and the 50–230 keV electrons were released even later, at 10:26 UT, just a few minutes before the type IV emission tends to disappear. Thus it seems possible that the rising shock and/or the moving plasmoid changes the magnetic topology above the release site or gives rise to a shielding (storage and release) of the high-energy electrons. In this context it may be recalled that the type IV is observed already at 10:11 UT, i.e., during the second hard X-ray maximum at 10:14 UT. The type II emission starts a little later, at 10:15 UT, and ends after 10:22 UT.

It should be mentioned that the appearance/disappearance of the type II emission is controlled by the plasma parameters of the ambient corona. In a recently published paper Mann et al. (2003) analysed the formation and development of shock waves in the solar corona. These authors estimate the radial behaviour of the Alfvén velocity and they argue that this velocity has a local minimum in the order of 200–400 km s^{-1} between 0.2 and 0.4 $R_\odot$. This behaviour of the Alfvén speed allows to understand the first detection of the type II burst at a height of roughly 0.4 $R_\odot$ because the shock has its maximal strength, i.e., Alfvén-Mach number, at this radial distance. Above this region the Alfvén velocity increases again and reaches a value of 700–800 km s^{-1} at heights around 3.0 $R_\odot$ above the photosphere. Taking into consideration that the radial shock speed derived from the frequency drift is about 540 km s^{-1} it seems possible that the source speed becomes sub-Alfvénic, i.e., fast-mode shocks and type II radio emission should disappear.

Furthermore, one should recall that Simnett et al. (2002) favoring an acceleration of high-energy electrons by CME-driven shocks argue that the radial height at the electron release time is between 0.5 and 2.5 $R_\odot$ above the photosphere. These heights are possibly related to the location of the previously mentioned extrema of the Alfvén speed.

Thus we would finally like to discuss the possibility that the rising shock produces the high-energy electrons observed at *Wind*. Assuming a first order Fermi process we can estimate the acceleration time to nearly-relativistic energies. The key parameters in this estimation are the magnetic turbulence in the plasma around the shock and the injection rate of pre-accelerated electrons. The magnetic turbulence increases with increasing Alfvén-Mach number of the shock and the acceleration process requires an injection energy larger than v_A for protons and $\sqrt{(m_\mathrm{p}/m_\mathrm{e})}v_\mathrm{A}$ for electrons (Melrose 1994). Assuming an Alfvén speed of 400 km s^{-1} the injection energy corresponding to this velocity is roughly 1 keV. Taking into consideration that the shock develops during the hard X-ray maximum around 10:14 UT there should be enough electrons with energies above the pre-acceleration threshold. According to Melrose (1994) typical acceleration times to nearly relativistic energies are smaller than 1 s. This means that the shock generating the type II emission should also be able to accelerate high-energy electrons shortly after the first type II emission at 10:15 UT. But this is not in agreement with our estimation of a first electron injection after the end of the type II emission, i.e., later than 10:22 UT.

Thus, the generation of the highly energetic electrons detected at *Wind* by a coronal shock wave is challenged again by the fact that the injection of these electrons is delayed with respect to the presumed acceleration time. This discrepancy was already mentioned by Klassen et al. (2002). Thus this situation is still puzzling and maybe the disappearance of the type II emission comes into play here. In this respect it may be recalled that the type II emission starts again after 10:30 UT. A possible explanation might be related to a change in the shock geometry affecting both type II emission and electron acceleration time or efficiency.

4. Summary and conclusions

Our study comprises various manifestations of the C8.0 flare on 2002 June 02 (10:05–10:30 UT). Both remotely detected electromagnetic emission and in situ measurements of highly energetic electrons were analysed using data with a high temporal resolution. The relative timing of the different flare manifestations was used to recapitulate the complex chronology of this particular event. In this context it should be realized that the results obtained here are the outcome of a detailed case-study and allow no offhand generalization.

The primary energy release is studied in hard X-rays (lightcurves and images) and microwaves (dynamic spectra). The RHESSI lightcurves consist of two maxima around 10:08 UT and 10:14 UT followed by a smooth decrease in the photon count rates. The photon count rates at higher energies (25–50 KeV) show a series of more or less well pronounced minor peaks with a temporal distance of roughly 1 min. The radio spectra from 0.8–4.5 GHz (observatory Ondřejov) comprise a series of fast drifting bursts with a close temporal association to the hard X-ray peaks.

The dynamic spectra from 40–800 MHz (Potsdam observatory) show a well-defined type IV burst starting around 10:11 UT and a series of weak type III bursts around 10:12 UT. A second group of type III bursts at 10:14:20 UT indicates high-energy electrons ($\beta \approx 0.13$, i.e., $\epsilon \approx 4$ keV) on open field lines at this time. There is type II emission starting after 10:15 UT and ceasing at 10:22 UT. After 10:15 UT there is a close temporal association between minor hard X-ray peaks and fast drifting emission features associated with the type IV burst. The radio images from the Nançay Radioheliograph show that the type IV source is moving outward with a velocity of roughly 450 km s^{-1}. The type II producing shock wave is clearly seen in front of the type IV source and has a radial speed of roughly 540 km s^{-1} indicating that the plasmoid is driving the shock.

First in situ measurements of high-energy electrons were recorded at *Wind* after 10:30 UT. The *Wind*/3-DP experiment detected electrons from 27–182 keV and our analysis revealed a relative injection at 10:22 UT for the lower energy electrons around 30 keV and 10:26 UT for the higher energy electrons, respectively. We find a good temporal association with minor hard X-ray peaks but not with the hard X-ray maxima. The electron injection definitely took place after the disappearance of the type II radio emission.

The delayed electron injection with respect to both maxima of primary energy release, i.e., hard X-ray maxima, *and* shock wave development, i.e., type II emission, gives rise to some implications concerning the electron acceleration and injection process. The magnetic connection between flare site and Earth seems to be established. There is evidence for energetic electrons on open field lines during the second hard X-ray maximum around 10:14 UT ($\epsilon \approx 4$ keV) and during minor peaks around 10:22 ($\epsilon \approx 30$ keV) and 10:26 UT ($\epsilon > 50$ keV). Only the last two groups of electron populations were definitively detected at *Wind*/3-DP. At these times there are also observations of microwave bursts and fast drifting type IV fine structures. This close temporal correlation with manifestations of an energy release in the lower corona suggests that the high-energy electrons detected at *Wind* have been accelerated in the reconnection scenario shortly described in the introduction. Although the temporal coincidence might be accidental (due to the uncertainties in the estimation of the electron injection time) the reconnection process is still in progress. Furthermore, we assume that the electron injection at an earlier time is shielded by the shock and the rising plasmoid or that they are giving rise to a storage and release of high-energy electrons.

In order to corroborate this scenario it would be essential to obtain electron spectra for the minor hard X-ray peaks and to include the propagation effects from the acceleration site to the spacecraft. It should be checked whether the high-energy electron populations generated during the primary energy release can explain the particle spectra recorded at *Wind*. In any case it should be kept in mind that the computation of an electron spectrum out of hard X-ray spectra requires additional assumptions to be non-ambiguous and that the analysis of propagation effects is complicated by the various processes described before.

Considering an electron acceleration at a rising shock in higher layers of the corona, say above 0.4 $R_\odot$, we face the following problem. If we assume that the electrons have been accelerated at the shock one has to explain an injection several minutes after an acceleration might have occurred. A First order Fermi process should be able to produce high-energy electrons a few seconds after the appearance of the type II, i.e., around 10:15 UT but the injection took place after the disappearance of the emission at 10:22 UT. We suggest that this behaviour could be explained by a change in the shock geometry. In any case we need some additional mechanism to explain the observed time delay.

Thus, for the high-energy electrons recorded at *Wind* on June 02 around 10:30 UT we argue in favor of an acceleration associated with the reconnection process taking place in the lower corona. The electron injection takes place after the disappearance of the type II emission. As seen in the microwave and hard X-ray emission there are clear indications of an ongoing reconnection process. This was not the case for the events studied by Klassen et al. (2002). For these events the injection took place while the type II emission was in progress and there were no indications of a reconnection process in the lower corona. Thus, it seems obvious that further investigations should look in particular at the relative timing of type II emission and electron injection.

Acknowledgements. The work of H. T. Claßen was supported by DLR under grant No. 50 QL 0001. The data and software for the hard X-ray and particle observations were provided by the RHESSI and Wind 3-D Plasma and Energetic Particle Investigation team (R. P. Lin, PI) at the University of California, Berkeley. The radio spectra of the observatory Ondřejov are by courtesy of Marian Karlický. The data and software for the radio images were provided by the Nançay Radioheliograph Group. Finally, the authors would like to thank Steven Kahler for lively and stimulating discussions.

References

Armstrong, T. P., Pesses, M. E., & Decker, R. B. 1985, Shock Drift Acceleration, in Collisionless Shocks in the Heliosphere: Reviews of Current Research, ed. B. T. Tsurutani, & R. G. Stone, (Washington DC: AGU Geophys. Monograph 35), 271

Bai, T., & Ramaty, R. 1979, ApJ, 227, 1072

Bai, T., & Dennis, B. 1985, ApJ, 292, 699

Claßen, H. T., & Aurass, H. 2002, A&A, 384, 1098

Claßen, H. T., Mann, G., Klassen, A., & Aurass, H. 2003, Hvar Obs. Bull., 27, 151

de Jager, C. 1969, Solar flares, properties and problems, in COSPAR Symposion on Solar Flares and Space Res., ed. C. de Jager, & Z. Švestka (Amsterdam: North-Holland), 1

de Jager, C., Kuijpers, J., Correira, E., & Kaufmann, P. 1987, Sol. Phys., 110, 317

Forman, M. A., & Webb, G. M. 1985, Acceleration of Energetic Particles, in Collisionless Shocks in the Heliosphere: A Tutorial Review, ed. R. G. Stone, & B. T. Tsurutani (Washington DC: AGU Geophys. Monograph 34), 91

Haggerty, D., & Roelof, E. 2002, ApJ, 579, 841

Heyvaerts, J. 1981, Particle Acceleration in Solar Flares, in Solar Flare Magnetohydrodynamics, ed. E. Priest (New York, London, Paris: Gordon and Breach), 429

Jiřička, K., Karlický, M., Kepka, O., & Tlamicha, A. 1993, Sol. Phys., 147, 203

Kerdraon, A., & Delouis, J.M. 1997, The Nançay Radioheliograph, in Lecture Notes in Physics 483, Coronal Physics from Radio and Space Observations, ed. G. Trottet (Berlin, Heidelberg, New York: Springer), 192

Klassen, A., Aurass, H., Klein, K.-L., Hofmann, A., & Mann, G. 1999, A&A, 343, 287

Klassen, A., Bothmer, V., Reiner, M. J., et al. 2002, A&A, 385, 1078

Krucker, S., Larson, D. E., Lin, R. P., & Thompson, B. J. 1999, ApJ, 519, 864

Lin, R. P., Anderson, K. A., Ashford, S., et al. 1995, Space Sci. Rev., 71, 125

Lin, R. P., Dennis, B. R., Hurford, G. J., et al. 2002, Sol. Phys., 210, 3

Mann, G., Aurass, H., Voigt, W., & Paschke, J. 1992, ESA SP-348, 129

Mann, G., Claßen, H. T., & Motschmann U. 2001, J. Geophys. Res., 106, 25, 323

Mann, G., Klassen, A., Aurass, H., & Claßen, H. T. 2003, A&A, 400, 329

Melrose, D. B. 1994, Kinetic Plasma Physics, in Plasma Astrophysics, ed. A. O. Benz, & T. J.-L. Courvoisier (Berlin, Heidelberg, New York: Springer), 113

Nelson, G. S., & Melrose, D. B. 1985, Type II Bursts, in Solar Radiophysics, ed. D. J. McLean, & N. R. Labrum (Cambridge: Cambridge Univ. Press), 333

Newkirk, G. Jr. 1961, ApJ, 133, 983

Priest, E. R. 1981, Current Sheets, in Solar Flare Magnetohydrodynamics, ed. E. Priest (New York, London, Paris: Gordon and Breach), 139

Stewart, R. T. 1985, Moving Type IV Bursts, in Solar Radiophysics, ed. D. J. McLean, & N. R. Labrum (Cambridge: Cambridge Univ. Press), 361

Simnett, G. M., Roelof, E. C., & Haggerty, D. K. 2002, ApJ, 579, 854

Sturrock, P. A., Kaufmann, P., Moore, R. L., & Smith, D. F. 1984, Sol. Phys., 94, 341

Suzuki, S., & Dulk, G. A. 1985, Bursts of Type III and Type V, in Solar Radiophysics, ed. D. J. McLean, & N. R. Labrum (Cambridge: Cambridge Univ. Press), 289

Švestka, Z. 1976, Particle Emission from Solar Flares, in Solar Flares, ed. Z. Švestka (Dordrecht, Boston: D. Reidel Publ. Co.), 260

Wild, J. P., Smerd, S. F., & Weiss, A. A. 1963, ARA&A, 1, 291